THE JOURNAL OF PHYSICAL CHEMISTRY C

Article

pubs.acs.org/JPCC

Molecular Characteristics of a Mixed-Valence Polyoxovanadate $\{V^{IV/V}_{18}O_{42}\}$ in Solution and at the Liquid–Surface Interface

Oliver Linnenberg,[†] Marco Moors,[‡] Albert Solé-Daura,[§] Xavier López,[§] Christoph Bäumer,[‡] Emmanuel Kentzinger,[∥] Wim Pyckhout-Hintzen,[⊥] and Kirill Yu. Monakhov*[,†]

[†]Institut für Anorganische Chemie, RWTH Aachen University, Landoltweg 1, 52074 Aachen, Germany

[‡]Peter Grünberg Institute (PGI), JARA-FIT, Forschungszentrum Jülich GmbH, Wilhelm-Johnen-Straße, 52425 Jülich, Germany

[§]Departament de Química Física i Inorgànica, Universitat Rovira i Virgili, c/Marcel·lí Domingo 1, 43007 Tarragona, Spain

[∥]Jülich Centre for Neutron Science (JCNS) and Peter Grünberg Institute (PGI), JARA-FIT, Forschungszentrum Jülich GmbH, Wilhelm-Johnen-Straße, 52425 Jülich, Germany

[⊥]Jülich Centre for Neutron Science (JCNS) and Institute for Complex Systems (ICS), Forschungszentrum Jülich GmbH, Wilhelm-Johnen-Straße, 52425 Jülich, Germany

Supporting Information

ABSTRACT: The understanding of the molecular state of vanadium-oxo clusters (polyoxovanadates, POVs) in solution and on surface is a key to their target application in catalysis as well as molecular electronics and spintronics. We here report the results of a combined experimental and computational study of the behavior of nucleophilic polyoxoanions $[V^{IV}_{10}V^{V}_{8}O_{42}(I)]^{5-}$ charged balanced by Et_4N^+ in water, a one-phase organic solution of *N*,*N*-dimethylformamid (DMF) or acetonitrile (MeCN), a mixed solution of MeCN–water, and at the hybrid liquid–surface interface. The molecular characteristics of the compound $(NEt_4)_5[V_{18}O_{42}(I)]$ (**1**) in the given environments were studied by microspectroscopic, electrochemical, scattering, and molecular mechanics methods. Contrary to the situation in pure water, where we observe great agglomeration with a number of intercalated H_2O molecules between POVs that are surrounded by the Et_4N^+ ions, no and only minor agglomeration of redox-active POVs in an unprecedented cation-mediated fashion was detected in pure DMF and MeCN, respectively. An inclusion of 1% water in the MeCN solution does not have an effect significant enough to reinforce agglomeration; however, this leads to the POV···POV interface characterized by the presence of the Et_4N^+ ions and a small number of H_2O molecules. Water amounts of ≥5% trigger the formation of higher oligomers. The deposition of compound **1** from MeCN onto an Au(111) surface affords nearly round-shaped particles (~10 nm). The use of DMF instead of MeCN results in bigger, irregularly shaped particles (~30 nm). This change of solvent gives rise to more extensive intermolecular interactions between polyoxoanions and their countercations as well as weaker binding of ion-pairing induced agglomerates to the metallic substrate. Lower concentration of adsorbed molecules leads to a submonolayer coverage and an accompanied change of the POV's redox state, whereas their higher concentration results in a multilayer coverage that offers the pristine mixed-valence structure of the polyoxoanion. Our study provides first important insights into the reactivity peculiarities of this redox-responsive material class on a solid support.

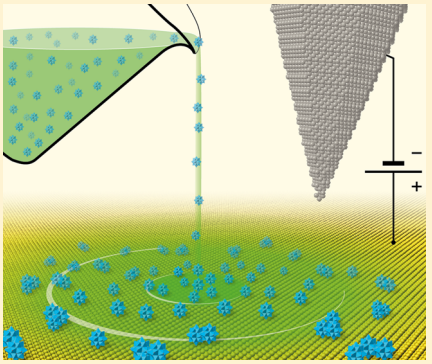

INTRODUCTION

Owing to the great potential to exploit their inherent properties in a unique combination (structure/charge/redox state/magnetic state/resistivity), reduced polyoxovanadate (POV) single molecules attract significant attention among experimentalists and theoreticians working in the field of polyoxometalates[1−6] (metal-oxo clusters, abbreviated as POMs), the latter find a wide range of applications from catalysis[7] to nanoelectronics.[8,9] The "fully-reduced" and mixed-valence POV structures are nowadays the subject of studies in biomedicine[10] as well as toward molecular quantum cellular automata,[11,12] "nanoscale quantum magnets", spin qubits, and spintronic devices.[13−16] Their target application in supported-POV heterogeneous catalysis[17−20] and in technologically relevant charge transport and optical mechanisms through individual, redox-responsive magnetic vanadium-oxo clusters,[21] however, requires control over the underlying characteristics and operation of these commonly negatively charged molecules in solution and on the substrate surface upon molecular deposition from the liquid phase.

Although the synthesis of POMs frequently occurs in an aqueous medium at controlled pH, in specific cases their direct microspectroscopic investigation[22−31] may mandate the use of an organic solvent. Indeed, an in-depth analysis of the

Received: March 6, 2017
Revised: April 12, 2017
Published: April 24, 2017

DOI: 10.1021/acs.jpcc.7b02138
J. Phys. Chem. C XXXX, XXX, XXX−XXX

hypersensitive relationships of nucleophilic POM structures with their charge-balancing cations[32] (quaternary ammonium cations, ionic liquid cations, and/or alkali metal cations) and solvent molecules may substantially facilitate effective and efficient implementation of POMs in devices of interest. The POM−counterion and POM−solvent interactions have far-reaching consequences for the structure−property relations and reactivity from the perspective of applied materials and surface science.

While ion-pairing[33] between POM anions[34] and their countercations[35] as well as defined aggregation[36] of individual POMs into hierarchical self-assemblies,[37] micelles or vesicles[38−41] have stood in the focus of intense experimental and computational investigations over the last 10 years, the details of POM−counterion/solvent interactions remain almost unexplored[42,43] for POVs. Additionally, the correlation between the aggregation or agglomeration behavior of the particles in solution and after adsorption on a metallic surface represents a new aspect of research in POM chemistry, which is crucial for the future integration of POMs in catalytic systems and the molecule-based electronic and spintronic devices. With the aim of providing insights into the behavior of a POV bulk sample in solution and on metallic surfaces, we probed the tetraethylammonium (TEA = Et_4N^+) salt of a mixed-valence, host−guest[44] vanadium-oxo cluster $[V^{IV}{}_{10}V^{V}{}_{8}O_{42}(I)]^{5-}$ (hereafter referred to as V_{18}) synthesized[45] by Müller and co-workers. Hereby, we set the focus on the agglomeration properties of this polyoxoanion in solvents with different polarity and after adsorption on the well-studied Au(111) model surface.

The interest in $[V^{IV}{}_{10}V^{V}{}_{8}O_{42}(I)]^{5-}$ containing reduced vanadyl $\{V^{IV}O\}^{2+}$ groups with isotropic spin 1/2 is triggered by its easy synthetic accessibility, thermodynamic stability, and potentially facile switching opportunities between V^{IV}/V^{V} ratios as indicated by an isostructural series of the host−guest polyoxoanions exhibiting a spherical $\{V_{18}O_{42}\}$ cluster shell (18:0 ("fully reduced"),[46] 16:2, and 10:8 (mixed valence)[45]). Moreover, the structural motif of V_{18} is archetypal for numerous semimetal-substituted POV materials[47] that take part in catalytic processes[48] and are characterized by intriguing magnetic properties.[47] The stability, redox activity, and the molecular state of the title $(NEt_4)_5[V_{18}O_{42}(I)]$ compound (**1**) in aqueous and organic solutions were studied by ultraviolet−visible (UV/vis) spectroscopy, cyclic voltammetry (CV), small-angle X-ray scattering[49,50] (SAXS), and molecular dynamics (MD) simulations. The molecular characteristics of this compound deposited from solution on the Au(111) surface were analyzed by scanning tunneling microscopy (STM) and X-ray photoelectron spectroscopy (XPS).

EXPERIMENTAL AND COMPUTATIONAL METHODS

Synthesis of Compound 1. The synthesis of compound **1** was performed according to the published method by Müller et al.[45] The molecular composition and the purity of crystalline compound **1** were confirmed by standard elemental analysis, powder X-ray diffraction (Figure S1), and infrared spectroscopy (IR) (see the Supporting Information).

Small Angle X-ray Scattering (SAXS). SAXS experiments were performed on all samples (see Table 2) using GALAXI[51] at the Jülich Centre for Neutron Science, Forschungszentrum Jülich. The wavelength of X-ray radiation from a liquid GaInSn target was 0.134 nm. Detector distances of approximately 3.5 and 0.8 m were used to yield a Q-range from 0.05 to 6 nm^{-1}. Q is the scattering vector and is defined as $(4\pi/\lambda)\sin(\vartheta/2)$, where ϑ is the scattering angle. The two-dimensional detector (Pilatus 1M) data were corrected for capillary scattering and scaled to absolute intensity $[cm^{-1}]$ through the scattering of a secondary polymer standard film (Fluoro-ethylene-propylene, Dupont) previously calibrated to water at the ID02 SAXS diffractometer of the ESRF, Grenoble, France. Before this, the data were azimuthally averaged using FIT-2D of ESRF. The samples were sealed in quartz capillaries of 1.5 mm inner diameter, placed in the vacuum chamber, and measured at ambient temperature. Solvents were treated in the same way and were subtracted from the data, weighted with their volume fraction. Since the Q-range overlap of both detector distances coincided in the peaked region (vide infra), for the subsequent fitting only the shorter detector distance was used without loss of information or generality.

Molecular Dynamics (MD) Simulations. MD simulations were carried out using GROMACS 4.5.4 software[52−54] and the AMBER 99 force field,[55] which has been successfully employed by Chaumont and Wipff[56−58] to study the aggregation of polyoxotungstates in solution. Parameters for the topology of the $[V^{IV}{}_{10}V^{V}{}_{8}O_{42}(I)]^{5-}$ polyoxoanion and the Et_4N^+ countercation, namely, V_{18} and TEA, respectively, were obtained following the procedure developed by Poblet and co-workers.[59,60] The structure of V_{18} was fully optimized using the Gaussian09 package[61] at the DFT level (BP86 functional)[62] and the LANL2DZ basis set.[63] For the organic TEA we used a Pople-type double-ζ basis set supplemented with polarization functions.[64−66] In addition, solvent effects were included during the geometry optimization using the dielectric IEF-PCM model.[67] CHelpG atomic charges were obtained by means of DFT single-point calculations in vacuum on the optimized structures at the same level of theory. Lennard-Jones parameters for O atoms belonging to the metal-oxo skeleton were taken from ref 59, and those for V atoms were taken from the UFF force field.[68] TIP3P water model[69] was used to represent solvent water molecules. MeCN and DMF were described by the models provided by van der Spoel et al.[70]

For the MD simulations, 10 V_{18} polyoxoanions were randomly embedded in a cubic solvent box in which 50 TEA countercations were inserted at random positions to preserve the electroneutrality of the whole system. For simulations in water, the box size was $(119.0\ Å)^3$ (54459 water molecules). For those in pure MeCN and DMF, the box size was $(118.4\ Å)^3$ (18151 and 12369 solvent molecules, respectively). In calculations on wet MeCN including 1% volume of water, the simulation box contained 17716 MeCN and 471 water molecules, and on those including 5% volume of water, the box contained 16382 MeCN and 2723 water molecules. In all cases the POV concentration ranges from 0.010 to 0.009 mol·L^{-1}. All simulations were performed with 3D-periodic boundary conditions using an atom cutoff of 14 Å for 1−4 van der Waals and of 10 Å for 1−4 Coulombic interactions and corrected for long-range electrostatics by using the particle−particle mesh Ewald (PME) summation method.[71] Five independent 5 ns dynamics were performed at 300 K starting with random velocities. The temperature was controlled by coupling the system to a thermal bath using the Berendsen algorithm[72] with a relaxation time of 0.1 ps to keep the canonical conditions (NVT) along the whole simulation. In simulations within an isothermal−isobaric (NPT) ensemble, the system was also coupled to a barostat using the Berendsen algorithm[72] with a relaxation time of 0.1 ps. Newton equations of motion were

DOI: 10.1021/acs.jpcc.7b02138
J. Phys. Chem. C XXXX, XXX, XXX−XXX

integrated using the leapfrog algorithm,[73] and a time step of 1 fs. Bonds involving H atoms were restrained by means of the LINCS algorithm.[74] Before the production runs, all the systems were equilibrated by 1000 steps of energy minimization followed by a 250 ps simulation at constant volume (NVT) fixing the solute. Then, a 250 ps NVT run was carried out with the solute relaxed, a 500 ps run at constant temperature (300 K) and pressure (1 atm) (NPT), and finally a last 250 ps run (NVT).

Surface Sample Preparation. The (111) oriented gold single crystal used for the adsorption experiments was purchased by MaTeck, Germany. The surface preparation was done in a separate ultrahigh vacuum (UHV) chamber by repeated cycles of neon ion sputtering ($I \approx 3$ μA at p(Ne) = 2 × 10^{-6} mbar) and subsequent annealing at 1000 K. The so-cleaned substrate was then transferred to ambient conditions for coating with 1 μL of a freshly prepared POV solution and afterward quickly retransferred into UHV. Dry MeCN and DMF were used as solvents. In both solvents a complete dissolving of compound **1** was observed, so that the given concentrations were directly calculated by the used quantity of the solid compound.

Scanning Tunneling Microscopy (STM). STM experiments were conducted under UHV conditions at room temperature in an Omicron VT-SPM. The base pressure inside the stainless steel vessel during operation was 5 × 10^{-10} mbar. For STM imaging, mechanically cut Pt−Ir tips were used. All images were measured in constant current mode. The SPIP 5.1.11 software from Image Metropolis was used for STM data analysis.

X-ray Photoelectron Spectroscopy (XPS). XPS measurements were performed with a PHI 5000 Versa Probe (Physical Electronics Inc., USA) with Al Kα X-ray illumination, a pass energy of 58.7 eV, and a photoemission angle of 55° using electron neutralization. The stainless steel vessel had a base pressure of 1 × 10^{-9} mbar. For binding energy reference, the C 1s peak at 285 eV was used. The spectra were fitted to a convolution of a Lorentz profile and a Gaussian profile after subtraction of a Shirley background.

RESULTS AND DISCUSSION

Structure and Redox Properties of V_{18}. The structure[45] of the herein studied host−guest V_{18} polyoxoanion is illustrated in Figure 1. It consists of the 18 self-assembled, edge-sharing square-pyramidal {O = VO_4} units shaping a spherical vanadium-oxo shell with a diameter of ca. 11 Å, which encapsulates an iodide ion (I^-) in the central void. The high negative charge of this POV component in compound **1** is counterbalanced by five TEA cations.

Because compound **1** shows good solubility in MeCN and DMF we spectroscopically tested the stability of V_{18} in these organic solvents and additionally under slightly harsher conditions, namely, in buffered aqueous solutions of HOAc/KOAc (OAc^- = acetate) in the range pH 3−6. A typical broad intervalence (V^{IV}/V^V) charge transfer (IVCT) band[75,76] at ca. λ_{max} = 920 nm has been observed in the UV/vis spectra of **1** in the specified solutions, thus demonstrating the mixed-valence character of V_{18}. Exception is the situation in the HOAc/KOAc medium at pH lower than 5 where the IVCT band does not appear, which indicates a degradation of the title POV (Figures S2−S4 in the Supporting Information). A comparative analysis between the solid-state IR spectrum of polycrystalline **1** and those spectra obtained after evaporation of the organic solutions of **1** under an ambient atmosphere (Figure S5 in the Supporting Information) suggests that the solid compound maintains its structural integrity after solvation in MeCN or DMF. In addition, the solid-state XPS spectrum of **1**, discussed below, confirms the mixed-valence form of the V_{18} polyoxoanion.

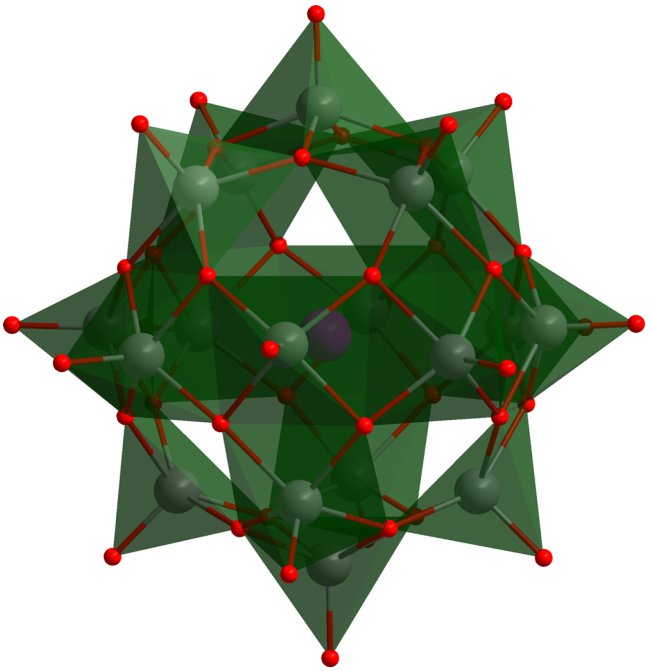

Figure 1. Combined ball-and-stick and polyhedral representation of a molecular structure of the spherical V_{18} polyoxoanion in compound **1**. Color code: V = gray spheres; O = red spheres; {VO_5} = transparent green square pyramids.

As a next step, we assessed the redox properties of the mixed-valence V_{18} polyoxoanion by CV measurements in a 0.1 M $TEAPF_6$−MeCN solution (T = 25 °C) for dE/dt = 20−200 mV·s^{-1} in the range of E = −2.43−0.67 V using the half-wave potential ($E_{1/2}$(Fc/Fc^+) = +0.380 V vs saturated calomel electrode)[77] of ferrocene/ferrocenium (Fc/Fc^+) as an external standard (see Figures S6−S8 in the Supporting Information). The main results of this electrochemical analysis are shown in Figure 2 and summarized in Table 1.

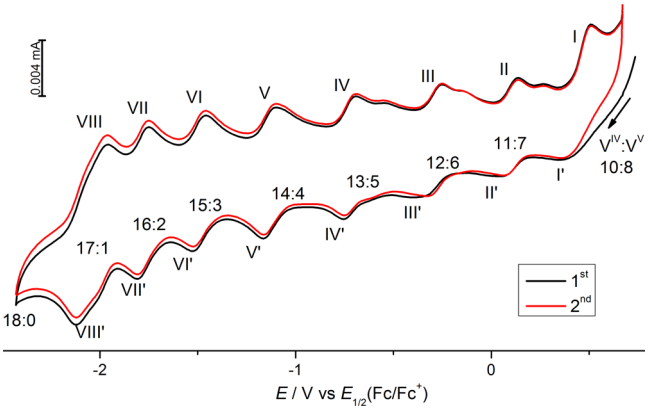

Figure 2. Cyclic voltammogram (1st and 2nd cycles) of compound **1** (0.3 mM) in a 0.1 M $TEAPF_6$−MeCN solution, with a scan rate of 50 mV·s^{-1} vs. Fc/Fc^+.

DOI: 10.1021/acs.jpcc.7b02138
J. Phys. Chem. C XXXX, XXX, XXX−XXX

Table 1. Data from Cyclic Voltammograms Presented in Figure 2 and Figures S6–S8 in the Supporting Information

	$E_{1/2}$ [V][a]		$\Delta E_{ox/red}$ [V]		i_{pc}/i_{pa}
dE/dt [mV·s^{-1}] =	50	100	50	100	50
I/I′	0.45	0.37	0.12	0.15	
II/II′	0.11	0.03	0.06	0.06	1.0
III/III′	−0.28	−0.35	0.06	0.06	1.0
IV/IV′	−0.72	−0.79	0.06	0.06	0.9
V/V′	−1.12	−1.20	0.06	0.06	0.9
VI/VI′	−1.48	−1.56	0.06	0.06	0.9
VII/VII′	−1.78	−1.85	0.06	0.06	1.0
VIII/VIII′	−2.04	−2.11	0.15	0.16	

[a]Solution of 0.3 mM in 0.1 M $TEAPF_6$-MeCN vs $E_{1/2}(Fc/Fc^+)$.

The first and second cycles depicted in the cyclic voltammogram (Figure 2) reveal a Coulomb staircase of eight reduction waves and the corresponding oxidation waves for dE/dt = 50 mV·s^{-1}, which reflect the maximum possible 8-fold one-electron reduction of V_{18} (that is $\{V^{IV}{}_{10}V^{V}{}_{8}\} \rightarrow \{V^{IV}{}_{18}V^{V}{}_{0}\}$) and the following reoxidation to the initial electron population, respectively. For E > 0.7 V the irreversible decomposition of compound **1** on the electrode surface is observed. This is in agreement with the fact that no isostructural $\{V_{18}O_{42}(X)\}$ complexes oxidized greater than V_{18} with V^{IV}/V^{V} = 10:8 could be obtained so far (see $\{V^{IV}{}_{18-n}V^{V}{}_{n}(X)\}$[45] where n = 0, 2, or 8 and X = anionic or neutral guest).

For waves II, III, and IV distinct shouldering effects in the anodic region are identifiable. These effects arose probably due to minor ion pairing hindering the oxidation of V_{18}. The peak-to-peak distances ($\Delta E_{ox/red}$ in Table 1) for the redox couples II/II′–VII/VII′ at two different scan rates (50 and 100 mV·s^{-1}) fit with the ideal value of $\Delta E_{ox/red}$ = 59 mV at 25 °C[78] for reversible one-electron transfers. The slight deviation from this value can be attributed to some uncompensated resistance.[9] This is also in accordance with the peak-current ratios (i_{pc}/i_{pa}) of II/II′–VII/VII′, which agree closely with the ideal value of 1;[78] minor differences may arise in consequence of kinetic limitation (refer to a transfer coefficient α > 0.5).[78] For the redox couples I/I′ and VIII/VIII′ the peak–current ratio could not be determined exactly. Furthermore, I/I′ and VIII/VIII′ exhibit much higher peak separations, which can be associated with an electrochemically irreversible but chemically reversible behavior or with a possible multiple electron transfer caused by adsorption on the cathode (VIII/VIII′) or convolution/superposition effects as a consequence of the irreversible decomposition on the anodic electrode surface (I/I′) at higher potentials. For all redox couples the peak height is proportional to the square root of the scan rate (see the Supporting Information), confirming an ideal diffusion-controlled behavior; although, a slight shift of $E_{1/2}$ to lower potentials is observed (see Table 1).

In comparison with CV measurements in MeCN, those in H_2O (conditions: 0.1 M KCl or $LiClO_4$ electrolyte; Ag/AgCl reference electrode; glassy carbon working electrode; platinum wire counter electrode) did not show any discrete redox waves. This can have several possible causes such as strong agglomeration or protonation effects.

It is also noteworthy that the determination of diffusion coefficients and hydrodynamic radii for compound **1** in MeCN via standard dynamic light scattering techniques has failed, in particular because of the absorption of laser light (λ = 632 nm) lying in the broad IVCT region of V_{18} (see the Supporting Information). We therefore sought further details of the solution behavior of compound **1** by SAXS.

SAXS Measurements. The SAXS data covered length scales up to a few tens of nanometers. Due to the peaked structure they were interpreted in terms of intraparticle (form factor $P(Q)$) and interparticle (structure factor $S(Q)$) correlations. For the shape of the V_{18} polyoxoanions a rotationally averaged spherical geometry (see Figure 1) was assumed. The scattering length density was calculated from the electron density of V_{18} by applying the gross formula in which the bulk density of 1.91 g·cm^{-3} was used. Tabulated densities for the respective calculation for MeCN and DMF were used. With the squared difference of scattering length density between these two components, that is the contrast $\Delta\rho^2$ and the volume fraction in the dilute solution of ∼1 mg·mL^{-1} in DMF, both the Q-dependence yielding the radius R_p of the spherical entity as well as the volume of the scattering particle V_p from the extrapolated experimental forward scattering $I(Q = 0)$ are in accordance within better than 10% with a monomeric V_{18} conformation. This agreement can be judged excellent given the experimental uncertainties in concentrations, densities, absolute calibration, and capillary scattering subtractions. At this concentration, the data can thus be interpreted directly as $P(Q)$, the form factor of the V_{18} polyoxoanions. We note that the countercation TEA cannot be distinguished from either DMF or water and thus the pure anionic vanadium-oxo cluster is determined. In MeCN a small contribution of the shell could be expected, however, leading to a larger effective particle radius. At a 10-fold higher concentration in DMF as well as in mixed solvents of MeCN and water, the SAXS data show an additional broad peaked intensity pattern around $Q \approx$ 0.9 nm^{-1} indicative for a Bragg-like peak or from a liquid-like ordering, which must be described by an appropriate structure factor $S(Q)$. The latter reduces to 1 if the vanadium-oxo clusters are dilute and do not experience the presence of neighboring clusters. Although they are charged species but are complexed with counterions, an effective hard-sphere potential is assumed here for the interaction.[79] This potential has been shown previously[80] to be a good approximation for both soft matter and hard matter systems. Due to its analytical form it provides an ideal way to parametrize the scattering data. Thus, the intensity curves $I(Q)$ were fitted with $I(Q) = \phi\Delta\rho^2 V_p P(Q,R_p)S(Q,R_{HS},\eta)$. Here, the volume V_p is calculated from the particle radius R_p, and the effective interaction hard sphere R_{HS} with an effective volume fraction η can be viewed as half the distance D between the centers-of-mass of interacting V_{18} polyoxoanions. This D can be roughly estimated already from the relation $D \approx 2\pi/Q_{peak}$. The formal expressions for $P(Q)$ and $S(Q)$ along with some more details (Figure S9) are given in the Supporting Information. In the fitting an additional diffuse background contribution due to closeness of the amorphous halo was taken into account. The fits are shown in Figure 3. The agreement is good and the small remaining discrepancies are assigned to the monodisperse and simple-spherical assumption of V_{18} as well as to details of the interaction potential. In reality this is presumably softer and should resemble more to a screened Coulomb dependence. However, because we are interested here merely in the question of monomeric or oligomeric vanadium-oxo clustering, the parametrization that focuses on the intercluster distance is sufficient.

The measured SAXS data show a weak dependence of the V_{18} polyoxoanion sphere size from the used solvent. The R_p

DOI: 10.1021/acs.jpcc.7b02138
J. Phys. Chem. C XXXX, XXX, XXX–XXX

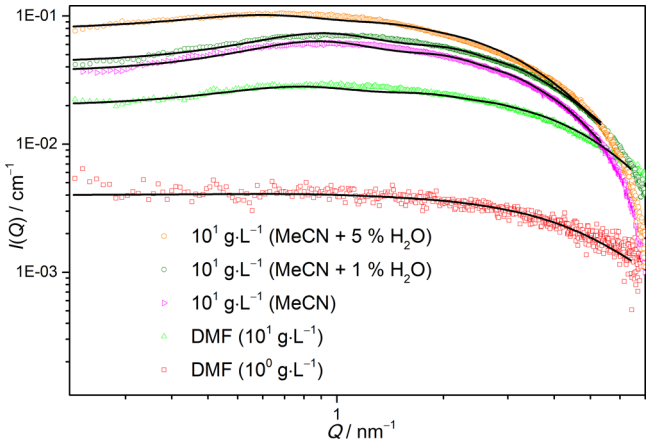

Figure 3. Absolute SAXS intensity data $I(Q)$ (in cm^{-1}) and corresponding fits to a spherical form factor and simulated hard-sphere interaction as a function of the scattering vector Q (in nm^{-1}). The compound concentration of 1 $g{\cdot}L^{-1}$ allows the form factor to be determined, whereas higher concentrations reveal non-negligible interactions. Due to the smallness of the particle, no oscillations of the form factor are observed, and the data are almost entirely in the Guinier regime.

value of 0.63 nm in MeCN in comparison to 0.49 nm in DMF (Table 2) indicates a larger average particle size in the less polar

Table 2. SAXS Data and Modeling Shown in Figure 3[a]

solvent (concentration)	additional water content [%]	R_p [nm]	D [nm]
DMF (1×10^0 $g{\cdot}L^{-1}$)	0	0.49	6.10
DMF (1×10^1 $g{\cdot}L^{-1}$)	0	0.49	6.94
	0	0.63	6.24
MeCN (1×10^1 $g{\cdot}L^{-1}$)	1	0.63	6.06
	5	0.72	8.44

[a]Error bars are of the order of 0.1%.

medium, which might be explained by either a small cation shell contribution or a weaker charge compensation of MeCN. Ion pairing effects might be favored due to a larger shielding effect of the solvent. However, both values are in the range of mainly monomeric polyoxoanions with only very few amount of slightly larger particles.

Small water contents in the MeCN solvent in the range of 1% simulating typical wet solvents have no detectable influence on the particle size (Table 2). However, water amounts of 5% or greater result in a further increase of R_p indicating more and/or higher oligomers. This interpretation is also supported by the significantly increased average interparticle distance D. The formation of larger V_{18} agglomerates reduces the effective amount of isolated scattering centers in the solution so that the distance between them has to increase at the same time.

MD Simulations. The collected SAXS data prompted us to conduct MD simulations to obtain more detailed information about the characteristics of V_{18} in solution. The computations were performed in pure water (solvent in the synthesis of V_{18}), pure MeCN, pure DMF, and wet MeCN containing 1% volume of water, which represents the moisture that dry, high-purity organic solvent could take during the experimental setups. To explore the effect of including higher amounts of water in the organic solvent we also performed simulations in wet MeCN containing 5% volume of water. The main computational results reflecting the behavior of V_{18} in the above-mentioned solvents are shortly described as two important features (see Figure 4): the radial distribution functions (RDFs) between

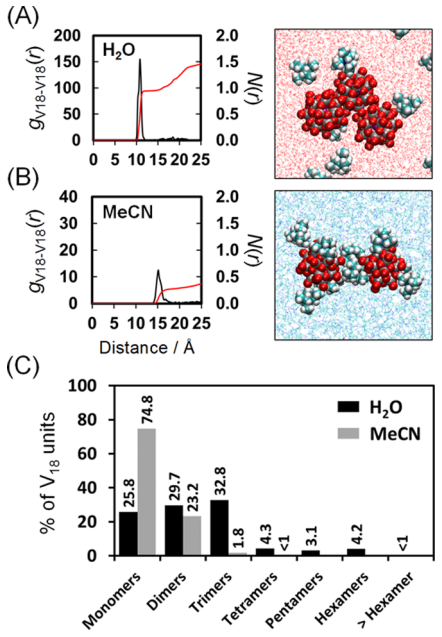

Figure 4. $V_{18}\cdots V_{18}$ RDFs between centers of mass (black curves) and typical snapshots of the agglomerate species resulted from simulations of V_{18} in H_2O (A) and pure MeCN (B). Red lines represent the integration of the RDFs (g), that is the coordination number N(r), which indicates the average number of neighboring molecules. Color code: V = gray spheres; O = red spheres; N = blue spheres; C = cyan spheres; H = white spheres. Summary of the % of POV units forming each different agglomeration state species averaged over 25 ns of MD trajectories in H_2O (black bars) or MeCN (gray bars) is given in (C).

$V_{18}\cdots V_{18}$ centers of mass, both in pure H_2O and MeCN, accompanied by representative snapshots and the % of isolated monomers and oligomers detected in the MD runs. In addition, Table S1 in the Supporting Information summarizes the data obtained from the RDF analysis of the studied systems.

Simulations of V_{18} in Water. Visual inspection of the MD trajectories reveals, in addition to the presence of free monomers, agglomeration of V_{18} units to form mainly dimers and trimers, but also higher oligomers, in agreement with the lack of discreteness observed in the redox CV waves of compound **1** in water. Related to this, $V_{18}\cdots V_{18}$ interactions are much longer-lived than $V_{18}\cdots$TEA ones. In fact, the $V_{18}\cdots$TEA contacts that can be detected involve one or two TEA molecules per POV at the most and exist only during short time intervals, whereas most of the $V_{18}\cdots V_{18}$ agglomerates formed last for the rest of the simulation. The $V_{18}\cdots V_{18}$ RDF, illustrated in Figure 4A, displays a single sharp peak at ca. 10.8 Å (roughly the sum of two V_{18} radii) integrating to 0.94 V_{18} units. This is the average number of POVs surrounding another during the computed trajectories. It must be pointed out that TEA cations are partially hydrophobic, but not enough to form a microphase, as has been observed for the bulkier n-Bu_4N^+ cations.[56] Thus, V_{18} agglomeration occurs in a water-mediated fashion, consisting of POV$\cdots(H_2O)_x\cdots$POV patterns with a number of intercalated water molecules between POV units that are weakly surrounded by the TEA countercations. This pattern is also explained by the high POV$\cdots H_2O$ affinity

DOI: 10.1021/acs.jpcc.7b02138
J. Phys. Chem. C XXXX, XXX, XXX−XXX

(interaction energy of −1387 kJ·mol^{-1} per POV molecule, see Table 3). Indeed, the coordination number obtained from the integration of the first peak in V_{18}···TEA RDF (displayed in Figure S10) quantifies an average of 0.33 TEA cations in close contact with each V_{18} unit. We expect the first shell of water molecules surrounding POVs not to be easily displaced to form agglomerates. In solution, TEA ions mediating POV···POV agglomerates were not observed at least for the present simulation time, but this possibility cannot be discarded completely. Results on longer simulation times are underway and will be published elsewhere.

Table 3. Interaction Energies[a] (E_{int}) Obtained from MD Simulations per POV Unit and per TEA Unit, Respectively

type of interaction	E_{int} [kJ·mol^{-1}]
POV···H_2O	−1387
POV···DMF	−735
POV···MeCN	−560
TEA···H_2O	−88
TEA···DMF	−129
TEA···MeCN	−111

[a]Averaged noncovalent intermolecular energies calculated from values taken every 2 ps over a total simulation time of 25 ns.

From MD trajectories, agglomeration is accounted for when the distance between the centers of mass of V_{18} units is <13 Å. Thus, 25.8% of the V_{18} units in solution remain as monomers, while agglomerates are represented mainly by dimers (29.7%) and trimers (32.8%), but also higher oligomers (4.3% of POVs being tetramers and the remaining 7.4% pentamers and hexamers). These data are summarized in Figure 4C. In total, ca. 74% of the V_{18} polyoxoanions form some type of agglomerate along the simulation time at 0.01 M concentration, certainly subscribing the notable tendency of V_{18} to form agglomerates in water.

Simulations of V_{18} in Pure MeCN and Pure DMF. With either solvent, visual inspection of the MD trajectories suggests strongly mitigated agglomeration with respect to the results in aqueous solution. In MeCN we mainly observe the presence of monomolecular V_{18} species with the exception of sparse formation of dimers. In solvents other than water, the agglomeration process occurs in an unprecedented and intricate cation-mediated POV···$(TEA)_x$···POV fashion. Consequently, the first peak in the corresponding V_{18}···V_{18} RDF (Figure 4B) appears at a larger distance of ca. 15.1 Å and integrates only to 0.25 V_{18} (vs 0.94 in H_2O).

Thus, larger POV···TEA ion pairing is expected in less polar organic solvents (see Figure S10 in the Supporting Information, which compares the V_{18}···TEA RDFs computed in H_2O, DMF, and MeCN). The basis for this is simply that the POV···solvent interaction is much weaker in organic solvents (see Table 3). Not only does the solvent polarity play a role but other sources of TEA···solvent affinity, such as dispersion or van der Waals interactions, can play a crucial role in limiting or aiding POV··· TEA pairing. In the present case, TEA has more affinity to DMF, −129 kJ·mol^{-1}, than to MeCN, −111 kJ·mol^{-1} (values shown in Table 3). This fact is ascribed to the role of the two methyl groups in DMF. We suggest, then, that the dipolar moment of the two organic solvents play a secondary role in the different behavior in solution since they are alike.

In MeCN, despite the considerable POV···TEA pairing computed (4.58 TEA per POV unit), the amount of V_{18} agglomeration is quite small (~25% vs ~74% in water; see Figure 4C), that is, the majority of POVs in this solvent remain monomeric (74.8%). In DMF, the V_{18}···V_{18} RDF (Figure S11 in the Supporting Information) does not show any definite and unambiguous peak, suggesting a complete lack of agglomeration. In this case, the TEA···DMF and POV···DMF affinities (−129 and −735 kJ·mol^{-1}, respectively), stronger compared with the ones in MeCN, derive from a lack of the necessary POV···TEA pairing for agglomeration, which explains this result. These findings fully agree with the SAXS data and with the observation of the well-defined redox peaks obtained from CV experiments in MeCN solution, confirming that V_{18} chiefly remains monomolecular.

Simulations of V_{18} in Wet MeCN. Results in wet MeCN (1% volume of water) do not show clear differences in comparison with results in pure MeCN. A single peak at ca. 14.7 Å is observed in the V_{18}···V_{18} RDF, integrating to 0.33 V_{18} (Figure S12A in the Supporting Information). This indicates that moisture in the solvent does not increase the tendency of V_{18} to form agglomerates. We assume that our trajectories are long enough for this comparative study since several randomly chosen water molecules were able to explore a large part of the space (Figure S13 in the Supporting Information). Also, the V_{18}···water RDF (Figure S12A in the Supporting Information) shows two peaks corresponding to the water molecules interacting with bridging and terminal atoms of the POV, respectively. This further demonstrates that water molecules reach the V_{18} units during the simulations. In the given case, the V_{18}···V_{18} agglomerates are mediated by TEA cations as in the previous section but we can also identify some water-mediated interactions as shown in a typical snapshot of a POV···$(TEA, H_2O)_x$···POV dimer in Figure S12A (Supporting Information). This combination of TEA and water molecules at the POV··· POV interface in wet MeCN seems to be responsible for the shorter V_{18}···V_{18} distance at the maximum of the peak in the RDF compared to that in pure MeCN. Nevertheless, when increasing the amount of water to 5%, we observe that the agglomeration slightly increases, as the peak in the corresponding V_{18}···V_{18} RDF (Figure S12B in the Supporting Information) integrates to 0.41 V_{18} (cf. 0.33 in simulations with 1% water). As the water molecules in the media tend to distribute around the POV (see V_{18}···H_2O RDF in Figure S12B), the larger number of agglomerate species must be a consequence of a higher number of water-mediated V_{18}···V_{18} contacts, as shown in Figure S14 (Supporting Information). This fact might explain the larger R_P observed for the 5% water-containing MeCN solution during SAXS measurements.

Molecular Surface Deposition and Characterization by STM. The use of combined redox, magnetic, and resistive properties of mixed-valence POVs in heterogeneous catalysis and in future single molecule-based nanoelectronic and nanospintronic devices mandates the controlled immobilization of these vanadium-oxo clusters onto a solid substrate. Therefore, we targeted the molecular deposition of V_{18} on the Au(111) surface from the liquid phase, which represents a first fundamental task in the technologically relevant multistep process. The substrate was chosen because of its well-investigated structure and easy preparation.[81] In order to stabilize the highly negatively charged V_{18} molecules without forming a huge solvent cloud we used the polar aprotic, dry solvents MeCN and DMF.

Figure 5A shows a representative STM image of the Au(111) surface, which was covered by a highly diluted V_{18}−MeCN

DOI: 10.1021/acs.jpcc.7b02138
J. Phys. Chem. C XXXX, XXX, XXX−XXX

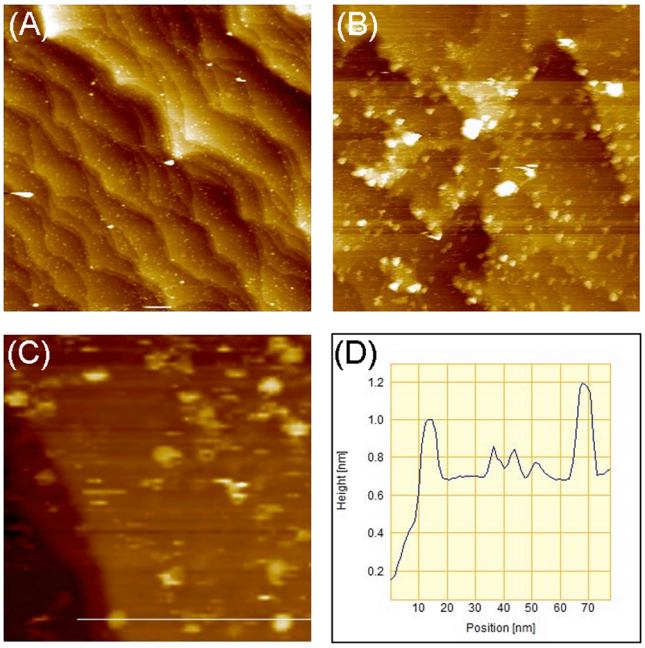

Figure 5. STM images of a submonolayer V_{18} covered Au(111) surface prepared by deposition (A) from a MeCN solution (concentration = 0.9 × 10^{-3} g·L^{-1}; 1000 nm × 1000 nm; U_B = 1.5 V, I_T = 0.5 nA) and (B) from a DMF solution (concentration = 1.4 × 10^{-3} g·L^{-1}; 900 nm × 900 nm; U_B = 1.5 V, I_T = 0.5 nA). Deposition from DMF solution results in bigger agglomerates and a preferred adsorption at the step edges of the substrate terraces. (C) High resolution scan of (A) (100 nm × 100 nm; U_B = 1.5 V, I_T = 0.5 nA). (D) Height profile from (C) along two presumable V_{18} polyoxoanions and some fragments.

solution with a concentration of compound **1** equal to 0.9 × 10^{-3} g·L^{-1}. Under these conditions a submonolayer coverage of nearly round shaped particles with a typical lateral diameter of ≈10 nm and a height ranging from 0.3 to 0.6 nm is found on most parts of the sample surface (see Figures 5C,D). Based on their characteristic size and reproducible shape we suppose that these particles may represent single V_{18} polyoxoanions, which are agglomerated through their TEA countercations. The adsorbed particles show no obvious ordering on the surface. A special preference of terrace step edges or other surface defects is not detected in that case. Besides these characteristic particles also a lot of smaller species with a less defined structure can be observed on the surface. If these objects refer to V_{18} fragments and/or solvent residues remains speculative.

Using DMF with a slightly higher polarity (polarity index[82] of 6.4 vs 5.8) and a much higher boiling point (153 °C vs 81.6 °C) than MeCN changes the V_{18} appearance on the Au(111) surface significantly. Figure 5B shows an STM image of a submonolayer covered sample area deposited from a V_{18}−DMF solution with a concentration of compound **1** equal to 1.4 × 10^{-3} g·L^{-1}. Compared to the situation after deposition from the MeCN solution the observed particles are much larger with an averaged lateral size of ∼30 nm and heights between 1.5 and 6 nm. The particles have no regular shape anymore and are obviously preferred located at the terrace step edges of the gold surface. This indicates the formation of larger agglomerates of several V_{18} polyoxoanions and their corresponding counterions due to more extensive intermolecular interactions (that is ion pairing), which, however, weakens the binding to the metallic substrate.

Thus, it gets obvious that the used solvent has a strong influence on the V_{18} adsorption behavior. We believe that the significantly higher boiling temperature of DMF compared to that of MeCN could be crucial for the larger agglomeration on the gold surface. The longer evaporation time of the solvent after the surface coating might lead to a higher surface mobility during the preparation process, but also polarity effects cannot be excluded although the SAXS measurements have shown an opposite trend for the polyoxoanion agglomeration in solution.

It should be noted that STM measurements of the adsorbed V_{18} polyoxoanions turned out to be quite challenging. Probably due to the high molecular charge of V_{18} interactions with the STM tip appeared quite frequently. Scanning with negative bias voltage (that is, with a positively charged tip) was hardly possible due to attraction of the negatively charged V_{18} molecules. Another problem, which was encountered during the measurements, was a somehow nonuniform V_{18} distribution on the macroscopic scale. Adjacent to the above-mentioned and mainly observed regions with submonolayer coverage also areas without V_{18} and other regions with multilayer coverage were found on the gold surface. We assume that the observed nonuniform distribution may be the result of an inhomogeneous evaporation of the solvent droplet during the deposition process since our SAXS measurements indicate no significant V_{18} agglomeration in the organic liquid phase. However, using MeCN as medium polar solvent with a low evaporation temperature enabled us to isolate small particles on the Au(111) surface, which should consist of only very few or even single V_{18} polyoxoanions. Further experiments with less polar solvents as well as the usage of other deposition techniques will be part of future studies.

XPS Data. The electronic properties of the V_{18} polyoxoanions adsorbed on the Au(111) surface were investigated by XPS as a function of solvent and concentration. For the measurements two significant solution concentrations of compound **1** were used: a lower concentration of 1.6 × 10^{-3} g·L^{-1}, which is in the range of our STM measurements showing a submonolayer coverage, and a higher concentration of 1.6 × 10^{-2} g·L^{-1} resulting in a multilayer coverage. For comparison also a solid-state XPS spectrum of the pure, unsolved V_{18} material was recorded. Figure 6 shows the corresponding binding energy region for the O 1s, V $2p_{1/2}$, and V $2p_{3/2}$ core levels. After background subtraction three groups of peaks are visible in the interesting binding energy region between 510 and 540 eV, which can be assigned to different oxygen and vanadium species.

At highest energies, oxygen 1s peaks can be found at 532.0 and 530.0 eV, respectively. While the sharper peak at lower energy can be clearly assigned to oxygen of V_{18}, the significantly broader peak is located in the typical range of surface adsorbates like hydroxide and carbonate species, which is characteristic for ex situ prepared samples. At low V_{18} concentration this component dominates the core level spectra. The two other groups of peaks belong to the $2p_{1/2}$ and $2p_{3/2}$ features of different vanadium species.[83] While the peaks at 524.2 and 516.7 eV can be assigned to fully oxidized V^V, partly reduced V^{IV} appears at 523.0 and 515.5 eV, respectively. For the unmodified V_{18} structure we would expect a V^{IV} to V^V ratio of 10:8. The measured relative vanadium contents based on the integration of the $2p_{3/2}$ peak intensities show for the bulk measurement and both solvents with the higher V_{18} concentration a slight excess of V^{IV} within the expected range indicating mainly unmodified V_{18} polyoxoanions (Table 4).

DOI: 10.1021/acs.jpcc.7b02138
J. Phys. Chem. C XXXX, XXX, XXX−XXX

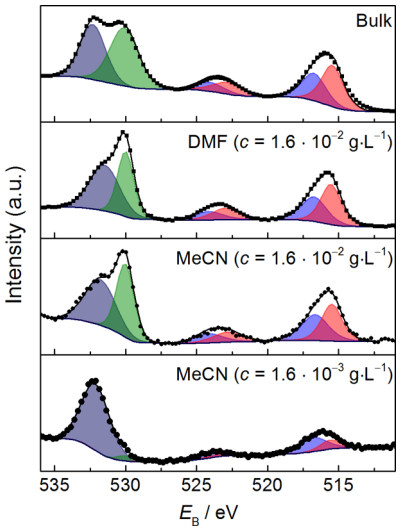

Figure 6. XPS spectra of the bulk V_{18} sample and a V_{18} covered Au(111) surface prepared by deposition from DMF or MeCN solution with different concentration of compound **1**. Peak fitting results in two O 1s peaks at 532.0 eV (gray curve) and 530.0 eV (green curve). Additionally, two different V species, V^{V} (blue curve) and V^{IV} (red curve), are detected with fitted $2p_{1/2}$ peaks at 524.2 and 523.0 eV, and $2p_{3/2}$ peaks at 516.7 and 515.5 eV, respectively.

Table 4. Data from XPS Spectra Shown in Figure 6

solvent (concentration)	vanadium $2p_{3/2}$	fitted peak position [eV]	relative vanadium content [%]
bulk	V^{IV}	515.4	7.0
	V^{V}	516.7	5.1
DMF (1.6×10^{-2} g·L^{-1})	V^{IV}	515.5	7.9
	V^{V}	516.7	5.9
MeCN (1.6×10^{-2} g·L^{-1})	V^{IV}	515.5	6.6
	V^{V}	516.7	6.0
MeCN (1.6×10^{-3} g·L^{-1})	V^{IV}	515.6	2.3
	V^{V}	516.7	4.8

The ratio changes drastically for the lower V_{18} concentration toward a higher amount of V^{V}. Although in this case the results should be interpreted with caution due to the overall low vanadium signal intensity, this observation indicates a partly oxidation of the mixed-valence V_{18} polyoxoanions on the surface.

The change in the vanadium ratios might be explained by the different binding situation of the V_{18} polyoxoanions on the gold surface. Using a concentration of 10^{-3} g·L^{-1} leads to a submonolayer coverage as shown by the STM measurements. Thus, most V_{18} polyoxoanions have direct contact to the metallic substrate, which induces a change of the POV's redox state by a charge transfer process. Using a higher concentrated solution of 10^{-2} g·L^{-1} for deposition results in a multilayer coverage, where the majority of the V_{18} polyoxoanions has no direct contact to the metal, so that their electronic structure remains unaffected.

CONCLUSIONS

By combining physical and chemical methods with locally resolved surface science techniques and MD simulations, it was possible to link the behavior of a highly charged V_{18} POV in solution and after adsorption on a metallic surface. Hereby, we demonstrated that the proneness of POVs to agglomerate in the liquid phase is strongly dependent on the polyoxoanion··· polyoxoanion interface that is governed by the solution medium (water vs organic solvent vs a mixture of water and organic solvent). The role of the countercation···solvent affinity in such agglomeration processes should not be neglected. Remarkably, the ion-pairing induced agglomeration of the V_{18} POVs increases significantly upon molecular deposition of the bulk sample **1** from organic solution onto the Au(111) surface. The size and shape of agglomerates and the strength of their binding to the metallic substrate are controlled by the physical properties such as polarity and boiling temperature of the organic solvent (MeCN vs DMF). While the solvent polarity and the resulting charge stabilization is decisive for agglomeration in solution, this effect is subordinated for the adsorption behavior. In that case, surface mobility is the key factor for agglomeration, which can be enhanced by a lower evaporation speed of the solvent. A higher amount of available hydrogen ions as a function of the water content increases the agglomeration tendency of the vanadium-oxo clusters in solution at higher water concentrations. Small water impurities, caused, for example, by humidity, have no significant influence.

These observations provide guidelines for fine-tuning the POV-surrounding (counterions and solvent molecules) relationships in solution as well as for the adjustment of the molecular adsorption on surfaces, which furthermore may open doors for potential photoluminescent effects[84,85] of POV particles on a solid support. This is worth further exploring because we have shown that the electronic structure of adsorbed POVs on the metallic surface undergoes redox modifications by the alteration of the molecule concentration-modulated surface coverage. Thus, it can be concluded that the interaction with the surface strongly influences the redox activity of the V_{18} polyoxoanions, which was detected by our CV measurements for the quasi-isolated vanadium-oxo clusters in solution.

The high complexity between the POV behavior in solution and on surfaces as shown in our study remains a key challenge for the utilization of this highly promising material class. The thermal controlled deposition on surfaces will be another logical step in order to fathom the possibilities for integrating POVs in real catalytic systems and technological devices. This is currently being explored in our laboratories.

ASSOCIATED CONTENT

Supporting Information

The Supporting Information is available free of charge on the ACS Publications website at DOI: 10.1021/acs.jpcc.7b02138.

Experimental data of compound **1** including elemental analysis, powder X-ray diffractogram, UV/vis and IR spectra, cyclic voltammograms, and additional SAXS data; details of MD calculations (PDF)

AUTHOR INFORMATION

Corresponding Author

*E-mail: kirill.monakhov@ac.rwth-aachen.de.

ORCID

Christoph Bäumer: 0000-0003-0008-514X

Kirill Yu. Monakhov: 0000-0002-1013-0680

Notes

The authors declare no competing financial interest.

DOI: 10.1021/acs.jpcc.7b02138
J. Phys. Chem. C XXXX, XXX, XXX−XXX

■ ACKNOWLEDGMENTS

This work was supported by the Emmy Noether program of the Deutsche Forschungsgemeinschaft (DFG). K.Y.M. and M.M. are grateful to the Jülich-Aachen Research Alliance—Future Information Technology (JARA-FIT) for a Seed Fund grant. X.L. gratefully acknowledges the European Science Foundation (PoCheMon COST action) for funding of a short-term scientific mission at the RWTH Aachen University, the Government of Catalonia (project 2014SGR199), and the Spanish Ministerio de Ciencia e Innovación (project CTQ2014-52774-P). We also thank Prof. Dr. Claire Besson (Department of Chemistry, The George Washington University) for helpful discussions and suggestions.

■ REFERENCES

(1) Pope, M. T.; Müller, A. Polyoxometalate Chemistry: An Old Field with New Dimensions in Several Disciplines. *Angew. Chem., Int. Ed. Engl.* **1991**, *30*, 34—48.

(2) Long, D.-L.; Burkholder, E.; Cronin, L. Polyoxometalate Clusters, Nanostructures and Materials: From Self Assembly to Designer Materials and Devices. *Chem. Soc. Rev.* **2007**, *36*, 105—121.

(3) Long, D.-L.; Tsunashima, R.; Cronin, L. Polyoxometalates: Building Blocks for Functional Nanoscale Systems. *Angew. Chem., Int. Ed.* **2010**, *49*, 1736—1758.

(4) Ammam, M. Polyoxometalates: Formation, Structures, Principal Properties, Main Deposition Methods and Application in Sensing. *J. Mater. Chem. A* **2013**, *1*, 6291—6312.

(5) See a themed collection on "Polyoxometalate Cluster Science": Cronin, L.; Müller, A. From Serendipity to Design of Polyoxometalates at the Nanoscale, Aesthetic Beauty and Applications. *Chem. Soc. Rev.* **2012**, *41*, 7333—7334.

(6) *Trends in Polyoxometalates Research*; Ruhlmann, L., Schaming, D., Eds.; Nova Science Publishers: Hauppauge, 2015.

(7) Wang, S.-S.; Yang, G.-Y. Recent Advances in Polyoxometalate-Catalyzed Reactions. *Chem. Rev.* **2015**, *115*, 4893—4962.

(8) Vilà-Nadal, L.; Mitchell, S. G.; Markov, S.; Busche, C.; Georgiev, V.; Asenov, A.; Cronin, L. Towards Polyoxometalate-Cluster-Based Nano-Electronics. *Chem. - Eur. J.* **2013**, *19*, 16502—16511.

(9) Busche, C.; Vilà-Nadal, L.; Yan, J.; Miras, H. N.; Long, D.-L.; Georgiev, V. P.; Asenov, A.; Pedersen, R. H.; Gadegaard, N.; Mirza, M. M.; et al. Design and Fabrication of Memory Devices Based on Nanoscale Polyoxometalate Clusters. *Nature* **2014**, *515*, 545—549.

(10) Postal, K.; Maluf, D. F.; Valdameri, G.; Rüdiger, A. L.; Hughes, D. L.; de Sá, E. L.; Ribeiro, R. R.; de Souza, E. M.; Soares, J. F.; Nunes, G. G. Chemoprotective Activity of Mixed Valence Polyoxovanadates against Diethylsulphate in *E. coli* Cultures: Insights from Solution Speciation Studies. *RSC Adv.* **2016**, *6*, 114955—114968.

(11) Tsukerblat, B.; Palii, A.; Clemente-Juan, J. M.; Coronado, E. Mixed-Valence Molecular Four-Dot Unit for Quantum Cellular Automata: Vibronic Self-Trapping and Cell-Cell Response. *J. Chem. Phys.* **2015**, *143*, 134307.

(12) Palii, A.; Tsukerblat, B. Tuning of Quantum Entanglement in Molecular Quantum Cellular Automata Based on Mixed-Valence Tetrameric Units. *Dalton Trans.* **2016**, *45*, 16661—16672.

(13) Kögerler, P.; Tsukerblat, B.; Müller, A. Structure-Related Frustrated Magnetism of Nanosized Polyoxometalates: Aesthetics and Properties in Harmony. *Dalton Trans.* **2010**, *39*, 21—36.

(14) Clemente-Juan, J. M.; Coronado, E.; Gaita-Ariño, A. Magnetic Polyoxometalates: From Molecular Magnetism to Molecular Spintronics and Quantum Computing. *Chem. Soc. Rev.* **2012**, *41*, 7464—7478.

(15) Monakhov, K. Y.; Linnenberg, O.; Kozłowski, P.; van Leusen, J.; Besson, C.; Secker, T.; Ellern, A.; López, X.; Poblet, J. M.; Kögerler, P. Supramolecular Recognition Influences Magnetism in $[X@HV^{IV}_{8}V^{V}_{14}O_{54}]^{6-}$ Self-Assemblies with Symmetry-Breaking Guest Anions. *Chem. - Eur. J.* **2015**, *21*, 2387—2397.

(16) Linnenberg, O.; Kozłowski, P.; Besson, C.; van Leusen, J.; Englert, U.; Monakhov, K. Y. A V_{16}-Type Polyoxovanadate Structure with Intricate Electronic Distribution: Insights from Magnetochemistry. *Cryst. Growth Des.* **2017**, DOI: 10.1021/acs.cgd.6b01397.

(17) Kholdeeva, O. A.; Maksimchuk, N. V.; Maksimov, G. M. Polyoxometalate-Based Heterogeneous Catalysts for Liquid Phase Selective Oxidations: Comparison of Different Strategies. *Catal. Today* **2010**, *157*, 107—113.

(18) Ren, Y.; Wang, M.; Chen, X.; Yue, B.; He, H. Heterogeneous Catalysis of Polyoxometalate Based Organic—Inorganic Hybrids. *Materials* **2015**, *8*, 1545—1567.

(19) Ye, J.-J.; Wu, C.-D. Immobilization of Polyoxometalates in Crystalline Solids for Highly Efficient Heterogeneous Catalysis. *Dalton Trans.* **2016**, *45*, 10101—10112.

(20) Soriano-López, J.; Goberna-Ferrón, S.; Vigara, L.; Carbó, J. J.; Poblet, J. M.; Galán-Mascarós, J. R. Cobalt Polyoxometalates as Heterogeneous Water Oxidation Catalysts. *Inorg. Chem.* **2013**, *52*, 4753—4755.

(21) Monakhov, K. Y.; Moors, M.; Kögerler, P. Perspectives for Polyoxometalates in Single-Molecule Electronics and Spintronics. *In Polyoxometalate Chemistry*; van Eldik, R., Cronin, L., Eds.; Advances in Inorganic Chemistry; Academic Press/Elsevier: Amsterdam, 2017; Vol. *69*, pp 251—286.

(22) Song, I. K.; Kaba, M. S.; Coulston, G.; Kourtakis, K.; Barteau, M. A. Scanning Tunneling Microscopy of Ordered Arrays of Heteropolyacids Deposited on a Graphite Surface. *Chem. Mater.* **1996**, *8*, 2352—2358.

(23) Song, I. K.; Kitchin, J. R.; Barteau, M. A. $H_3PW_{12}O_{40}$-Functionalized Tip for Scanning Tunneling Microscopy. *Proc. Natl. Acad. Sci. U. S. A.* **2002**, *99*, 6471—6475.

(24) Song, I. K.; Kaba, M. S.; Barteau, M. A. Nanoscale Investigation of Mixed Arrays of Keggin-Type and Wells—Dawson-Type Heteropolyacids (HPAs) by Scanning Tunneling Microscopy (STM). *Langmuir* **2002**, *18*, 2358—2362.

(25) Kim, J.; Gewirth, A. A. Interactions between the Keggin-Type Lacunary Polyoxometalate, α-$SiW_{11}O_{39}^{8-}$, and Electrode Surfaces. *Langmuir* **2003**, *19*, 8934—8942.

(26) Kim, J.; Lee, L.; Niece, B. K.; Wang, J. X.; Gewirth, A. A. Formation of Ordered Multilayers from Polyoxometalates and Silver on Electrode Surfaces. *J. Phys. Chem. B* **2004**, *108*, 7927—7933.

(27) Song, I. K.; Kaba, M. S.; Nomiya, K.; Finke, R. G.; Barteau, M. A. Scanning Tunneling Microscopy (STM) and Tunneling Spectroscopy (TS) Studies of Polyoxometalates (POMs) of the Wells—Dawson Structural Class. *J. Mol. Catal. A: Chem.* **2007**, *262*, 216—226.

(28) Alam, M. S.; Dremov, V.; Müller, P.; Postnikov, A. V.; Mal, S. S.; Hussain, F.; Kortz, U. STM/STS Observation of Polyoxoanions on HOPG Surfaces: the Wheel-Shaped $[Cu_{20}Cl(OH)_{24}(H_2O)_{12}(P_8W_{48}O_{184})]^{25-}$ and the Ball-Shaped $[\{Sn(CH_3)_2(H_2O)\}_{24}\{Sn(CH_3)_2\}_{12}(A\text{-}PW_9O_{34})_{12}]^{36-}$. *Inorg. Chem.* **2006**, *45*, 2866—2872.

(29) Choi, J. H.; Park, D. R.; Park, S.; Song, I. K. Scanning Tunneling Microscopy and Tunneling Spectroscopy of Nano-structured $H_6P_2Mo_xW_{18-x}O_{62}$ (x = 0, 3, 9, 15, 18) Wells-Dawson Heteropolyacids. *J. Nanosci. Nanotechnol.* **2011**, *11*, 6533—6538.

(30) Zhong, D.; Sousa, F. L.; Müller, A.; Chi, L.; Fuchs, H. A Nanosized Molybdenum Oxide Wheel with a Unique Electronic-Necklace Structure: STM Study with Submolecular Resolution. *Angew. Chem., Int. Ed.* **2011**, *50*, 7018—7021.

(31) Lombana, A.; Rinfray, C.; Volatron, F.; Izzet, G.; Battaglini, N.; Alves, S.; Decorse, P.; Lang, P.; Proust, A. Surface Organization of Polyoxometalate Hybrids Steered by a 2D Supramolecular PTCDI/Melamine Network. *J. Phys. Chem. C* **2016**, *120*, 2837—2845.

(32) Watfa, N.; Melgar, D.; Haouas, M.; Taulelle, F.; Hijazi, A.; Naoufal, D.; Avalos, J. B.; Floquet, S.; Bo, C.; Cadot, E. Hydrophobic Effect as a Driving Force for Host—Guest Chemistry of a Multi-Receptor Keplerate-Type Capsule. *J. Am. Chem. Soc.* **2015**, *137*, 5845—5851.

DOI: 10.1021/acs.jpcc.7b02138
J. Phys. Chem. C XXXX, XXX, XXX—XXX

(33) Mei, Y.; Huang, W.; Yang, Z.; Wang, J.; Yang, X. Ion-Pairing and Aggregation of Ionic Liquid-Neutralized Polyoxometalate Salts in Aqueous Solutions. *Fluid Phase Equilib.* **2016**, *425*, 31−39.
(34) Pigga, J. M.; Kistler, M. L.; Shew, C.-Y.; Antonio, M. R.; Liu, T. Counterion Distribution around Hydrophilic Molecular Macroanions: The Source of the Attractive Force in Self-Assembly. *Angew. Chem., Int. Ed.* **2009**, *48*, 6538−6542.
(35) Antonio, M. R.; Nyman, M.; Anderson, T. M. Direct Observation of Contact Ion-Pair Formation in Aqueous Solution. *Angew. Chem., Int. Ed.* **2009**, *48*, 6136−6140.
(36) Lesage de la Haye, J.; Pontes da Costa, A.; Pembouong, G.; Ruhlmann, L.; Hasenknopf, B.; Lacôte, E.; Rieger, J. Study of the Temperature-Induced Aggregation of Polyoxometalate-poly(*N,N*-diethylacrylamide) Hybrids in Water. *Polymer* **2015**, *57*, 173−182.
(37) Izzet, G.; Abécassis, B.; Brouri, D.; Piot, M.; Matt, M.; Serapian, S. A.; Bo, C.; Proust, A. Hierarchical Self-Assembly of Polyoxometalate-Based Hybrids Driven by Metal Coordination and Electrostatic Interactions: From Discrete Supramolecular Species to Dense Monodisperse Nanoparticles. *J. Am. Chem. Soc.* **2016**, *138*, 5093−5099.
(38) Landsmann, S.; Wessig, M.; Schmid, M.; Cölfen, H.; Polarz, S. Smart Inorganic Surfactants: More than Surface Tension. *Angew. Chem., Int. Ed.* **2012**, *51*, 5995−5999.
(39) Bu, W.; Uchida, S.; Mizuno, N. Micelles and Vesicles Formed by Polyoxometalate−Block Copolymer Composites. *Angew. Chem., Int. Ed.* **2009**, *48*, 8281−8284.
(40) Pradeep, C. P.; Misdrahi, M. F.; Li, F.-Y.; Zhang, J.; Xu, L.; Long, D.-L.; Liu, T.; Cronin, L. Synthesis of Modular "Inorganic−Organic−Inorganic" Polyoxometalates and Their Assembly into Vesicles. *Angew. Chem., Int. Ed.* **2009**, *48*, 8309−8313.
(41) Li, D.; Yin, P.; Liu, T. Supramolecular Architectures Assembled from Amphiphilic Hybrid Polyoxometalates. *Dalton Trans.* **2012**, *41*, 2853−2861.
(42) Li, D.; Song, J.; Yin, P.; Simotwo, S.; Bassler, A. J.; Aung, Y.; Roberts, J. E.; Hardcastle, K. I.; Hill, C. L.; Liu, T. Inorganic−Organic Hybrid Vesicles with Counterion- and pH-Controlled Fluorescent Properties. *J. Am. Chem. Soc.* **2011**, *133*, 14010−14016.
(43) Li, D.; Liu, Z.; Song, J.; Li, H.; Zhang, B.; Yin, P.; Zheng, Z. N.; Roberts, J. E.; Tsige, M.; Hill, C. L.; et al. Cation Translocation around Single Polyoxometalate−Organic Hybrid Cluster Regulated by Electrostatic and Cation−π Interactions. *Angew. Chem., Int. Ed.* **2017**, *56*, 3294−3298.
(44) Müller, A.; Reuter, H.; Dillinger, S. Supramolecular Inorganic Chemistry: Small Guests in Small and Large Hosts. *Angew. Chem., Int. Ed. Engl.* **1995**, *34*, 2328−2361.
(45) Müller, A.; Sessoli, R.; Krickemeyer, E.; Bögge, H.; Meyer, J.; Gatteschi, D.; Pardi, L.; Westphal, J.; Hovemeier, K.; Rohlfing, R.; et al. Polyoxovanadates: High-Nuclearity Spin Clusters with Interesting Host−Guest Systems and Different Electron Populations. Synthesis, Spin Organization, Magnetochemistry, and Spectroscopic Studies. *Inorg. Chem.* **1997**, *36*, 5239−5250.
(46) Johnson, G. K.; Schlemper, E. O. Existence and Structure of the Molecular Ion 18-Vanadate(IV). *J. Am. Chem. Soc.* **1978**, *100*, 3645−3646.
(47) Monakhov, K. Y.; Bensch, W.; Kögerler, P. Semimetal-Functionalised Polyoxovanadates. *Chem. Soc. Rev.* **2015**, *44*, 8443−8483.
(48) Wendt, M.; Warzok, U.; Näther, C.; van Leusen, J.; Kögerler, P.; Schalley, C. A.; Bensch, W. Catalysis of "Outer-Phase" Oxygen Atom Exchange Reactions by Encapsulated "Inner-Phase" Water in $\{V_{15}Sb_6\}$-Type Polyoxovanadates. *Chem. Sci.* **2016**, *7*, 2684−2694.
(49) Nyman, M.; Fullmer, L. Small Angle X-ray Scattering of Group V Polyoxometalates. In *Trends in Polyoxometalates Research*; Ruhlmann, L., Schaming, D., Eds.: Nova Science Publishers: Hauppauge, 2015; pp 151−170.
(50) Nyman, M. Small-Angle X-Ray Scattering to Determine Solution Speciation of Metal-Oxo Clusters. *Coord. Chem. Rev.* **2016**.
(51) Kentzinger, E.; Krutyeva, M.; Rucker, U. Jülich Centre for Neutron Science. GALAXI: Gallium Anode Low-Angle X-Ray Instrument. *J. large-scale res. facilit* **2016**, *2*, A61.
(52) Hess, B.; Kutzner, C.; van der Spoel, D.; Lindahl, E. GROMACS 4: Algorithms for Highly Efficient, Load-Balanced, and Scalable Molecular Simulation. *J. Chem. Theory Comput.* **2008**, *4*, 435−447.
(53) van der Spoel, D.; Lindahl, E.; Hess, B.; Groenhof, G.; Mark, A. E.; Berendsen, H. J. C. GROMACS: Fast, Flexible, and Free. *J. Comput. Chem.* **2005**, *26*, 1701−1718.
(54) Berendsen, H. J. C.; van der Spoel, D.; van Drunen, R. GROMACS: A Message-Passing Parallel Molecular Dynamics Implementation. *Comput. Phys. Commun.* **1995**, *91*, 43−56.
(55) Wang, J. M.; Cieplak, P.; Kollman, P. A. How Well Does a Restrained Electrostatic Potential (RESP) Model Perform in Calculating Conformational Energies of Organic and Biological Molecules? *J. Comput. Chem.* **2000**, *21*, 1049−1074.
(56) Chaumont, A.; Wipff, G. Ion Aggregation in Concentrated Aqueous and Methanol Solutions of Polyoxometallates Keggin Anions: the Effect of Counterions Investigated by Molecular Dynamics Simulations. *Phys. Chem. Chem. Phys.* **2008**, *10*, 6940−6953.
(57) Chaumont, A.; Wipff, G. Do Keggin Anions Repulse Each Other in Solution? The Effect of Solvent, Counterions and Ion Representation Investigated by Free Energy (PMF) Simulations. *C. R. Chim.* **2012**, *15*, 107−117.
(58) Chaumont, A.; Wipff, G. Polyoxometalate Keggin Anions at Aqueous Interfaces with Organic Solvents, Ionic Liquids, and Graphite: a Molecular Dynamics Study. *J. Phys. Chem. C* **2009**, *113*, 18233−18243.
(59) Leroy, F.; Miró, P.; Poblet, J. M.; Bo, C.; Bonet Ávalos, J. Keggin Polyoxoanions in Aqueous Solution: Ion Pairing and Its Effect on Dynamic Properties by Molecular Dynamics Simulations. *J. Phys. Chem. B* **2008**, *112*, 8591−8599.
(60) López, X.; Nieto-Draghi, C.; Bo, C.; Avalos, J. B.; Poblet, J. M. Polyoxometalates in Solution: Molecular Dynamics Simulations on the α-$PW_{12}O_{40}^{3-}$ Keggin Anion in Aqueous Media. *J. Phys. Chem. A* **2005**, *109*, 1216−1222.
(61) Frisch, M. J.; Trucks, G. W.; Schlegel, H. B.; Scuseria, G. E.; Robb, M. A.; Cheeseman, J. R.; Scalmani, G.; Barone, V.; Mennucci, B.; Petersson, G. A.; et al. *Gaussian 09*, revision A.01; Gaussian, Inc.: Wallingford, CT, 2009.
(62) Becke, A. D. Density-Functional Exchange-Energy Approximation with Correct Asymptotic Behavior. *Phys. Rev. A: At., Mol., Opt. Phys.* **1988**, *38*, 3098−3100.
(63) Hay, P. J.; Wadt, W. R. *Ab Initio* Effective Core Potentials for Molecular Calculations. Potentials for the Transition Metal Atoms Sc to Hg. *J. Chem. Phys.* **1985**, *82*, 270−283.
(64) Francl, M. M.; Pietro, W. J.; Hehre, W. J.; Binkley, J. S.; Gordon, M. S.; DeFrees, D. J.; Pople, J. A. Self-Consistent Molecular Orbital Methods. XXIII. A Polarization-Type Basis Set for Second-Row Elements. *J. Chem. Phys.* **1982**, *77*, 3654−3665.
(65) Hehre, W. J.; Ditchfield, R.; Pople, J. A. Self-Consistent Molecular Orbital Methods. XII. Further Extensions of Gaussian-Type Basis Sets for Use in Molecular Orbital Studies of Organic Molecules. *J. Chem. Phys.* **1972**, *56*, 2257−2261.
(66) Hariharan, P. C.; Pople, J. A. The Influence of Polarization Functions on Molecular Orbital Hydrogenation Energies. *Theor. Chim. Acta* **1973**, *28*, 213−222.
(67) Cancès, E.; Mennucci, B.; Tomasi, J. A New Integral Equation Formalism for the Polarizable Continuum Model: Theoretical Background and Applications to Isotropic and Anisotropic Dielectrics. *J. Chem. Phys.* **1997**, *107*, 3032−3041.
(68) Rappe, A. K.; Casewit, C. J.; Colwell, K. S.; Goddard, W. A.; Skiff, W. M. UFF, a Full Periodic Table Force Field for Molecular Mechanics and Molecular Dynamics Simulations. *J. Am. Chem. Soc.* **1992**, *114*, 10024−10035.
(69) Jorgensen, W. L.; Chandrasekhar, J.; Madura, J. D.; Impey, R. W.; Klein, M. L. Comparison of Simple Potential Functions for Simulating Liquid Water. *J. Chem. Phys.* **1983**, *79*, 926−935.

DOI: 10.1021/acs.jpcc.7b02138
J. Phys. Chem. C XXXX, XXX, XXX−XXX

(70) Fischer, N. M.; van Maaren, P. J.; Ditz, J. C.; Yildirim, A.; van der Spoel, D. Properties of Organic Liquids when Simulated with Long-Range Lennard-Jones Interactions. *J. Chem. Theory Comput.* **2015**, *11*, 2938−2944.
(71) Darden, T.; York, D.; Pedersen, L. Particle Mesh Ewald: An *N*·log(*N*) Method for Ewald Sums in Large Systems. *J. Chem. Phys.* **1993**, *98*, 10089−10092.
(72) Berendsen, H. J. C.; Postma, J. P. M.; van Gunsteren, W. F.; DiNola, A.; Haak, J. R. Molecular Dynamics with Coupling to an External Bath. *J. Chem. Phys.* **1984**, *81*, 3684−3690.
(73) Hockney, R. W.; Goel, S. P.; Eastwood, J. W. Quiet High-Resolution Computer Models of a Plasma. *J. Comput. Phys.* **1974**, *14*, 148−158.
(74) Hess, B.; Bekker, H.; Berendsen, H. J. C.; Fraaije, J. G. E. M. LINCS: A Linear Constraint Solver for Molecular Simulations. *J. Comput. Chem.* **1997**, *18*, 1463−1472.
(75) Müller, A.; Meyer, J.; Bögge, H.; Stammler, A.; Botar, A. Trinuclear Fragments as Nucleation Centres: New Polyoxoalkoxyvanadates by (Induced) Self-Assembly. *Chem. - Eur. J.* **1998**, *4*, 1388−1397.
(76) Mondal, A.; Sarkar, S.; Chopra, D.; Guru Row, T. N.; Pramanik, K.; Rajak, K. K. Family of Mixed-Valence Oxovanadium(IV/V) Dinuclear Entities Incorporating N_4O_3-Coordinating Heptadentate Ligands: Synthesis, Structure, and EPR Spectra. *Inorg. Chem.* **2005**, *44*, 703−708.
(77) Pavlishchuk, V. V.; Addison, A. W. Conversion Constants for Redox Potentials Measured versus Different Reference Electrodes in Acetonitrile Solutions at 25°C. *Inorg. Chim. Acta* **2000**, *298*, 97−102.
(78) Zanello, P. Voltammetric Techniques. *In Inorganic Electrochemistry: Theory, Practice and Application* **2006**, 49−136.
(79) Percus, J. K.; Yevick, G. J. Analysis of Classical Statistical Mechanics by Means of Collective Coordinates. *Phys. Rev.* **1958**, *110*, 1−13.
(80) Kinning, D. J.; Thomas, E. L. Hard-Sphere Interactions between Spherical Domains in Diblock Copolymers. *Macromolecules* **1984**, *17*, 1712−1718.
(81) Barth, J. V.; Brune, H.; Ertl, G.; Behm, R. J. Scanning Tunneling Microscopy Observations on the Reconstructed Au(111) Surface: Atomic Structure, Long-Range Superstructure, Rotational Domains, and Surface Defects. *Phys. Rev. B: Condens. Matter Mater. Phys.* **1990**, *42*, 9307−9318.
(82) *Solvent Guide*; Burdick and Jackson Laboratories, 1984.
(83) Silversmit, G.; Depla, D.; Poelman, H.; Marin, G. B.; De Gryse, R. Determination of the V2p XPS Binding Energies for Different Vanadium Oxidation States (V^{5+} to V^{0+}). *J. Electron Spectrosc. Relat. Phenom.* **2004**, *135*, 167−175.
(84) Chen, L.; Jiang, F.; Lin, Z.; Zhou, Y.; Yue, C.; Hong, M. A Basket Tetradecavanadate Cluster with Blue Luminescence. *J. Am. Chem. Soc.* **2005**, *127*, 8588−8589.
(85) Chen, L.; Jiang, F.; Li, N.; Yan, C.; Xu, W.; Hong, M. Synthesis and Characterization of a Mixed-Valence Hexadecavanadate Cluster with Half-Open Framework. *Inorg. Chem. Commun.* **2009**, *12*, 219−222.

DOI: 10.1021/acs.jpcc.7b02138
J. Phys. Chem. C XXXX, XXX, XXX−XXX